Facile synthesis of silver-modified functionalised graphene oxide nanocomposite with enhanced antibacterial property

Menglong Wu[1], *Daban Lu*[2], *Yue Zhao*[1], *Tianzhen Ju*[1]

[1]*College of Geography and Environment Science, Northwest Normal University, Lanzhou, Gansu 730070, People's Republic of China*
[2]*College of Chemistry and Chemical Engineering, Lanzhou University, Lanzhou 730000, People's Republic of China*
E-mail: wml28@163.com

Published in Micro & Nano Letters; Received on 12th November 2012; Revised on 13th January 2013; Accepted on 15th January 2013

Silver nanoparticles (Ag NPs)-modified poly(diallyldimethylammonium chloride) (PDDA) functionalised graphene oxide (GO) nanocomposite was synthesised via a simple electrostatic attract assembly and used as an antibacterial material. The synthesised nanocomposite was characterised by UV–vis spectra, X-ray diffraction and transmission electron microscopy. The antibacterial properties of the nanocomposite were investigated against Gram-negative bacteria *Escherichia coli* and Gram-positive bacteria *Bacillus cereus*. The results showed that the nanocomposite displayed excellent antibacterial properties in comparison with Ag NPs, which is attributed to the synergistic effect of Ag NPs and the PDDA–GO sheets. Thus, the as-prepared nanocomposite in this study may be used as an effective antibacterial material.

1. Introduction: In recent years, nanosized metal particles as novel antimicrobial agents have been seen as promising candidates for application [1, 2]. In particular, silver nanoparticles (Ag NPs) show the most effective inhibitory and bactericidal properties and low cytotoxicity to human cells. Ag NPs themselves can directly damage the cytomembrane of bacteria, leading to impacts on permeability, and eventually result in cell death [3]. Nevertheless, the antibacterial activity of Ag NPs might be lost because of the existence of oxidation and aggregation. Therefore, to address these problems, a large number of materials have been employed as support materials to enhance the antibacterial activity and stability of Ag NPs [4–6].

Graphene, a monolayer of carbon atoms closely packed into honeycomb two-dimensional carbon material, has attracted great attention from both the experimental and the theoretical science communities [7]. At present, research attention has been drawn towards the antibacterial activity of graphene and its composite materials. Recent research reported that the graphene and graphene oxide (GO) suspensions could inhibit the growth of *Escherichia coli* (*E. coli*) bacteria but with a minimal cytotoxicity [8]. Ma *et al.* [9] reported that silver-modified GO nanosheets exhibited superior antibacterial activity towards *E. coli* because of the synergistic effect of GO and silver NPs. Therefore Ag–GO nanocomposites are supposed to be effective antibacterial materials, which possess the specific properties of both Ag NPs and GO, displaying excellent antibacterial properties.

A linear positively charged polyelectrolyte, poly(diallyldimethylammonium chloride) (PDDA) has been found to be an effective material to non-covalently functionalise graphene sheets through π–π interaction and electrostatic interaction. In addition, both *E. coli* and *Bacillus cereus* (*B. cereus*) cells were negatively charged under experimental conditions [9, 10]. Thus, the PDDA–GO might have stronger adsorption properties because of the positively charged capping polymers, and the bacterial cells could be adsorbed onto the nanocomposite surface, which increases the contact between the bacteria and the as-synthesised nanocomposite.

In this Letter, we report a facile method for the synthesis of Ag–PDDA–GO nanocomposite via electrostatic attract assembly. It is worth highlighting that our method can successfully anchor highly dispersed Ag NPs on GO sheets in the water system. Moreover, highly dispersed Ag NPs on GO supports with larger surface areas have advantages in antibacterial property. In addition, the antibacterial property of the Ag–PDDA–GO nanocomposite was then tested in detail against the Gram-negative bacteria *E. coli* and Gram-positive bacteria *B. cereus.* The bacteria were cultured both in bacterial growth medium and on agar plates. Experimental results showed that the Ag–PDDA–GO nanocomposites displayed excellent antibacterial properties. Therefore the nanocomposites have great potential as antibacterial materials.

2. Experimental

2.1. Materials: Graphite flake (nature, − 325 mesh) was purchased from Alfa Aesar (Beijing, China). PDDA (MW = 200 000–350 000) was from Sigma. Silver nitrate ($AgNO_3$) was obtained from the Tianjin Chemical Reagent Co. Ltd (China). Sodium borohydride ($NaBH_4$) and trisodium citrate dihydrate ($C_6H_5Na_3O_7{\cdot}2H_2O$) were from the Tianjin Guangfu Chemical Reagent Co. Ltd (China). All chemicals used for culturing of microorganisms were purchased from Beijing Shuangxuan Microbe Culture Medium Products Factory (China). All other reagents and solvents were of analytical grade and used without further purification. All chemicals were prepared with deionised water purified via Milli-Q unit.

2.2. Synthesis of the Ag–PDDA–GO nanocomposite: The citrate-stabilised Ag NPs were prepared according to a previously reported method [11]. Briefly, 50 ml $AgNO_3$ (0.02125 g) solution was mixed with 50 ml trisodium citrate (0.03676 g) solution under stirring. Then 0.5 ml of freshly prepared 0.2 M $NaBH_4$ was added dropwise into the above aqueous solution under vigorous stirring. The colour of the reaction mixture turns into yellow. After 30 min of stirring, the resulting silver solution was left undisturbed overnight.

GO was synthesised from natural graphite by using a modified Hummers and Offeman [12] method. In a typical procedure for the preparation of PDDA–GO, 100 ml yellow–brown dispersion of GO (0.5 mg/ml) was prepared by ultrasonication for 2 h, followed by centrifugation to remove any unexfoliated GO. Subsequently, the homogeneous GO dispersion was mixed with 2.5 ml PDDA solution (20%) and stirred for 30 min. The resulting composite was separated by centrifugation and further washed with water.

Ag NPs (5 mg) dispersed in deionised water (10 ml) was added into a 20 ml PDDA–GO water solution (0.5 mg/ml). After ultrasonication for 30 min, the mixture was kept stirred for 12 h at room

© The Institution of Engineering and Technology 2013

doi: 10.1049/mnl.2012.0872

temperature. Then the product was collected by centrifuge and washed with deionised water repeatedly.

2.3. Antibacterial test: Before each experiment, all glass apparatus and solutions used in the experiments were autoclaved at 121°C for 20 min to ensure sterility. Gram-negative bacterial strain, *E. coli* (ATCC 25922, supplied by the Guangzhou industry microbe test centre) and Gram-positive bacterial strain, *B. cereus* (WJ1, our lab) were chosen as the experimental strain for antibacterial activity experiments. *E. coli* was cultivated in Luria-Bertani medium and *B. cereus* was grown in nutrient broth at 37°C for 24 h with gentle shaking to obtain the exponential growth phase. Then $\sim 10^7$ cfu/ml bacteria cells were grown in 50 ml liquid medium supplemented with 0, 5, 10, 20 and 50 µg/ml of Ag NPs and Ag–PDDA–GO nanocomposite, and 0, 10, 20, 50 and 100 µg/ml of PDDA–GO, respectively. Growth rates and bacterial concentrations were determined by measuring the optical density at 600 nm (OD_{600}) using a UV–vis spectrophotometer based on the turbidity of the cell suspension every 2 h. To study further the antibacterial effect, *E. coli* and *B. cereus* cells were spread onto agar plates with bacterial suspensions and 50 µg/ml of Ag–PDDA–GO. The morphological changes of *E. coli* and *B. cereus* were investigated by scanning electron microscopy (SEM).

2.4. Characterisation techniques: UV–vis spectra were acquired with a uv-2102 (unico) UV–vis spectrometer (Shanghai, China). X-ray powder diffraction (XRD) patterns were recorded at room temperature, by D/max-2400 (Rigaku, Japan) using Cu-Kα radiation ($\lambda = 0.15418$ nm) and a 2θ scan rate of 10°/min. The diffraction patterns were taken over the 2θ range from 5° to 80°. Transmission electron microscopy (TEM) and high-resolution TEM (HRTEM) were carried out by a FEI Tecnai G^2 F30 instrument (USA) with an accelerating voltage of 200 kV. The powders were dispersed in deionised water before TEM characterisation. Field-emission SEM (FESEM) was performed on a Kevex JSM-6701 (Tokyo, Japan), operating at an accelerating voltage and applied current of 15 kV and 10 mA, respectively. The powders were coated with thin layers of gold before FESEM characterisation.

3. Results and discussion: The Ag–PDDA–GO nanocomposite was prepared by a simple procedure for assembly of the citrate-stabilised Ag NPs on the surface of PDDA–GO. The main steps are schematically illustrated in Fig. 1. The first step was the functionalisation of GO by PDDA. GO is the original basic material for the preparation of individual graphene sheets with abundant oxygen-containing surface functionalities, such as hydroxyl, carbonyl, carboxyl and epoxide groups. These groups allow GO sheets to have high water solubility and are negatively charged. Owing to the non-covalent adsorption of positively charged PDDA, the PDDA–GO was also positively charged. The citrate-stabilised Ag NPs were negatively charged and therefore electrostatically attracted to the surface of positively charged PDDA–GO. The large PDDA–GO sheets can act as an excellent

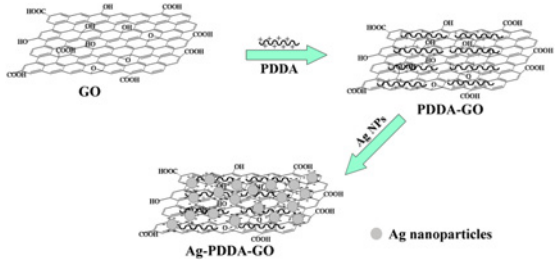

Figure 1 *Illustration of synthesis procedure of Ag–PDDA–GO nanocomposite*

support and stabiliser for the Ag NPs, avoiding nanoparticle aggregation.

Fig. 2*A* shows the UV–vis spectra of PDDA–GO, Ag NPs and Ag–PDDA–GO nanocomposite. The PDDA–GO dispersion (curve a) shows a strong absorption peak at 231 nm which referred to the π–π* transition of aromatic C = C bond and a shoulder peak at 300 nm which is attribute to the *n*–π* transition of the C = O bond. The as-prepared citrate-stabilised Ag NPs (curve b) display an absorption band at about 388 nm, which is the characteristic absorption band of Ag NPs caused by surface plasmon resonance. After the Ag NPs were deposited, the spectrum of the Ag–PDDA–GO nanocomposite (curve c) showed the characteristic peak of Ag NPs at 390 nm, which indicated the efficient adsorption of Ag NPs onto the PDDA–GO sheets surface.

Fig. 2*B* shows the XRD patterns of PDDA–GO and Ag–PDDA–GO nanocomposite. PDDA–GO (curve a) shows a strong peak centred at $2\theta = 10.6°$, corresponding to the (002) plane of GO. The diffraction peak at around 43° is associated with the (100) plane of the hexagonal structure of carbon. In curve b, the diffraction peaks at about 38.0°, 44.3°, 64.4° and 77.5° are in good agreement with the (111), (200), (220) and (311) crystallographic planes of face-centred cubic Ag NPs (JCPDS No. 87-0597), respectively. In addition, the characteristic peak of GO also appeared at about 10.6°. Therefore the as-synthesised Ag–PDDA–GO nanocomposite presents all diffraction peaks of the Ag NPs combined with GO. These results indicate that the Ag NPs are well loaded on the PDDA–GO sheets and the loading of Ag NPs does not affect the GO sheets packing from the layered structure during the experimental process.

The TEM image (Fig. 2*C*) shows that the wrinkled surface of the PDDA–GO has been decorated with Ag NPs and almost no Ag NPs are found outside of the PDDA–GO sheets, indicating a strong interaction between PDDA–GO substrate and the Ag NPs. Some NPs are slightly aggregated because of the loading degree close to saturation. Furthermore, owing to the large special surface areas of PDDA–GO sheets, the Ag NPs could be deposited on both sides of these sheets. Obviously, the Ag NPs of several nanometres diameter are loaded onto the surface of the PDDA–GO sheets. Some larger Ag NPs have a size of ~ 40 nm, and the size of the smaller ones was in the range of 4–25 nm with a

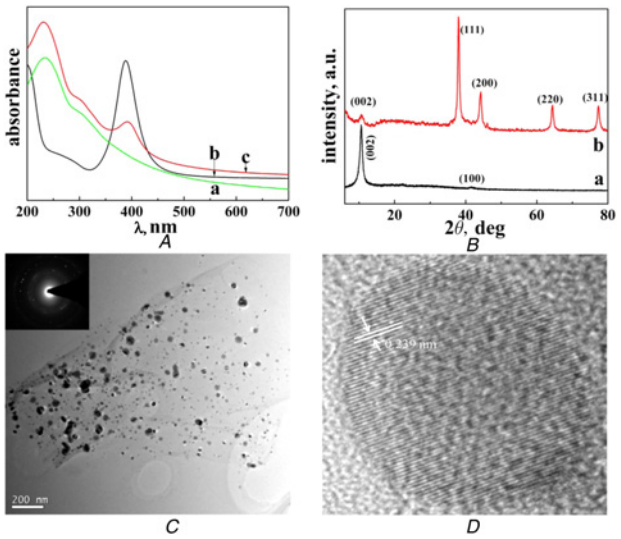

Figure 2 *UV–vis spectra; TEM image of Ag–PDDA–GO; HRTEM image of single Ag NP on PDDA–GO sheet*
A UV–vis spectra (a) PDDA–GO, (b) Ag NPs and (c) Ag–PDDA–GO
B XRD (a) PDDA–GO and (b) Ag–PDDA–GO
C TEM image of Ag–PDDA–GO. Inset: selected area electron diffraction pattern of Ag NPs
D HRTEM image of single Ag NP on PDDA–GO sheet

© The Institution of Engineering and Technology 2013

mean diameter of 8 nm. In addition, the selected area electron diffraction pattern of Ag NPs supported the formation of polycrystalline Ag NPs. The measured lattice-fringe spacing of the Ag NPs in the HRTEM image (Fig. 2*D*) is found to be 0.239 nm, which corresponds to the (111) crystal plane of Ag NPs [13].

The antibacterial activity of the Ag–PDDA–GO nanocomposite was evaluated by using Gram-negative bacteria *E. coli* and Gram-positive bacteria *B. cereus* as the bacterium model. The bacterial inhibition growth curve was used to investigate the bacterial growth kinetics and evaluate the antibacterial properties of the Ag–PDDA–GO nanocomposite. The bacterial growth was monitored by measuring the optical density at 600 nm (OD_{600}) based on the turbidity of the cell suspension. In Fig. 3, $\sim 10^7$ cfu/ml *E. coli* and *B. cereus* cells were grown in 50 ml liquid medium supplemented with certain concentration of PDDA–GO, Ag NPs and Ag–PDDA–GO nanocomposite. It can be seen in Figs. 3*a* and *d* that both *E. coli* and *B. cereus* have a robust growth of bacteria and no considerable antibacterial activity was observed for PDDA–GO, which confirms that PDDA–GO sheets have low toxicity to bacteria. Figs. 3*b* and *e* show that pure Ag NPs have effective antibacterial activity. One can clearly see that 87% of *E. coli* and 89% of *B. cereus* cells have been killed at the Ag NPs concentration of 20 μg/ml, and inhibited completely at the concentration of 50 μg/ml. Although, in comparison with the antibacterial behaviour of pure Ag NPs, the Ag–PDDA–GO nanocomposite illustrate the higher disinfection rate (Figs. 3*c* and *f*). The growth of bacteria was completely inhibited with Ag–PDDA–GO nanocomposite above a concentration of 20 μg/ml. These results obtained further confirmed that Ag–PDDA–GO composites have enhanced antibacterial activity compared with PDDA–GO and pure Ag NPs, which

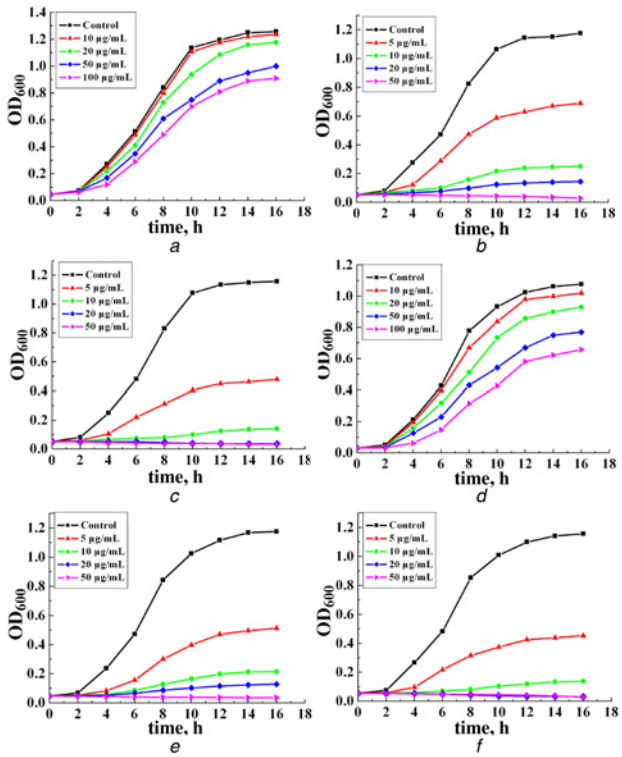

Figure 3 *Normalised bacterial growth curves for different materials*
E. coli
a PDDA–GO
b Ag NPs
c Ag–PDDA–GO
B. cereus
d PDDA–GO,
e Ag NPs
f Ag–PDDA–GO

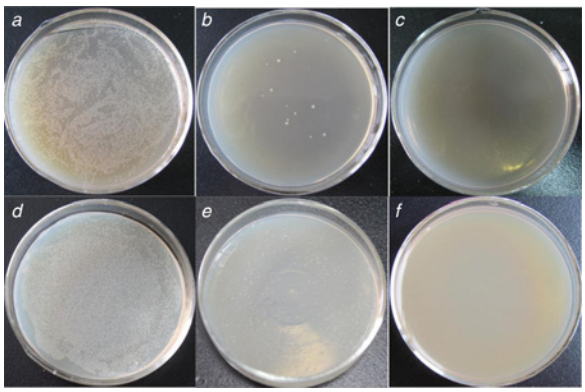

Figure 4 *Photographs of bacterial colonies formed by E. coli and B. cereus*
E. coli
a In the absence of Ag–PDDA–GO (control experiment) and treated with 50 μg/ml Ag–PDDA–GO for
b 5 min
c 10 min
B. cereus
d In the absence of Ag–PDDA–GO (control experiment) and treated with 50 μg/ml Ag–PDDA–GO for
e 5 min
f 10 min

is attributed to the synergistic antibacterial effect of Ag NPs and the PDDA–GO sheets. Ag NPs can interact with the sulphur-containing proteins of cell walls and phosphorus-containing compounds in cytoplasm and affect the function of cell respiration and cell division, resulting in the death of the bacteria [14]. On the other hand, the PDDA–GO has stronger adsorption properties because of the positively charged capping polymers, and the negatively charged bacterial cells could be adsorbed onto the nanocomposite surface, which increases the contact between the bacteria and the nanocomposite. In addition, pure Ag NPs might show lower antibacterial activity because of the aggregation during the antibacterial process, leading to the reduction of active specific surface area of Ag NPs. However, PDDA–GO was employed as support material to load Ag NPs to avoid aggregation, enhancing the stability of Ag NPs. Thus, the as-synthesised nanocomposite is effective antibacterial material, and the greater antibacterial property is attributed to the synergistic effect of Ag NPs and the PDDA–GO sheets.

The antibacterial effect was further confirmed by spreading *E. coli* and *B. cereus* cells onto agar plates with bacterial suspensions and 50 μg/ml of Ag–PDDA–GO nanocomposite. As can be seen from Fig. 4, the nanocomposite exhibited a very high antibacterial activity in a slurry system to both *E. coli* and *B. cereus*, with few colonies being able to form on the agar plate following a contact time of 5 min (Figs. 4*b* and *e*) compared with the blank sample (Figs. 4*a* and *d*), and no more cells were viable after 10 min (Figs. 4*c* and *f*).

The SEM was used to investigate the morphology of treated *E. coli* and *B. cereus* cells after disinfection. Fig. 5 reveals that

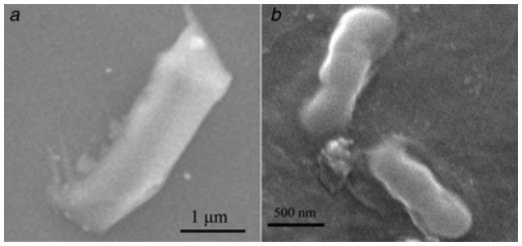

Figure 5 *SEM images of E. coli and B. cereus after being treated with Ag–PDDA–GO*
a E. coli
b B. cereus

© The Institution of Engineering and Technology 2013

doi: 10.1049/mnl.2012.0872

the Ag–PDDA–GO nanocomposite could obviously adsorb on the surface of the bacteria cells. Some research has also reported that GO sheets show high non-specific binding capability to microbes. Therefore the bacteria were wrapped by the Ag–PDDA–GO nanocomposite, which probably facilitated the direct contact of Ag NPs with the cell membranes. Then, Ag NPs can damage the cell wall when in contact with the bacteria. Eventually the bacteria can be destroyed into pieces. It can be clearly seen from Fig. 5*b* that the cell walls of the bacteria have been damaged significantly. The intact surfaces of the rod-like-shaped bacteria cells have been destroyed.

4. Conclusions: In this work, Ag–PDDA–GO nanocomposite was synthesised via a simple electrostatic attract assembly. The nanocomposite was characterised by UV–vis, XRD and TEM, which indicated that Ag NPs are loaded successfully on the surface of PDDA–GO. The nanocomposite display remarkably enhanced antibacterial capability towards *E. coli* and *B. cereus*, which is attributed to the synergistic antibacterial effect of stronger adsorption properties of positively charged PDDA–GO and the bactericidal property of Ag NPs. Therefore, the as-prepared nanocomposite in this study makes it reasonable to be used as an effective antibacterial material.

5. Acknowledgment: This work was supported by the National Natural Science Foundation of China (grant no. 41161080).

6 References

[1] Birringer R.: 'Nanocrystalline materials', *Mater. Sci. Eng*., 1989, **117**, pp. 33–43

[2] Liong M., France B., Bradley K.A., Zink J.I.: 'Antimicrobial activity of silver nanocrystals encapsulated in mesoporous silica nanoparticles', *Adv. Mater*., 2009, **21**, pp. 1684–1689

[3] Lalueza P., Monzon M., Arruebo M., Santamaria J.: 'Antibacterial action of Ag-containing MFI zeolite at low Ag loadings', *Chem. Commun*., 2011, **47**, pp. 680–682

[4] Gong P., Li H.M., He X.X., *ET AL*.: 'Preparation and antibacterial activity of Fe3O4@ Ag nanoparticles', *Nanotechnology*, 2007, **18**, 285604, pp. 1–7

[5] Shen J.F., Shi M., Li N., *ET AL*.: 'Facile synthesis and application of Ag-chemically converted graphene nanocomposite', *Nano Res*., 2010, **3**, pp. 339–349

[6] Santos C.M., Tria M.C.R., Vergara R.A.M.V., Ahmed F., Advincula R.C., Rodrigues D.F.: 'Antimicrobial applications of electroactive PVK-SWNT nanocomposites', *Chem. Commun*., 2011, **47**, pp. 8892–8894

[7] Geim A.K., Novoselov K.S.: 'The rise of graphene', *Nat. Mater*., 2007, **6**, pp. 183–191

[8] Hu W.B., Peng C., Luo W.J., *ET AL*.: 'Graphene-based antibacterial paper', *ACS Nano*, 2010, **4**, pp. 4317–4323

[9] Ma J.Z., Zhang J.T., Xiong Z.G., Yong Y., Zhao X.S.: 'Preparation, characterization and antibacterial properties of silver-modified graphene oxide', *J. Mater. Chem*., 2011, **21**, pp. 3350–3352

[10] Husmark U., Ronner U.: 'Forces involved in adhesion of *Bacillus cereus* spores to solid surfaces under different environmental conditions', *J. Appl. Bacteriol*., 1990, **69**, pp. 557–562

[11] Wei H., Chen C.G., Han B.Y., Wang E.K.: 'Enzyme colorimetric assay using unmodified silver nanoparticles', *Anal. Chem*., 2008, **80**, pp. 7051–7055

[12] Hummers W.S., Offeman R.E.: 'Preparation of graphitic oxide', *J. Am. Chem. Soc*., 1958, **80**, pp. 1339

[13] Pasricha R., Gupta S., Srivastava A.K.: 'A facile and novel synthesis of Ag-graphene-based nanocomposites', *Small*, 2009, **20**, pp. 2253–2259

[14] Schreurs W.J.A., Rosenberg H.: 'Effect of silver ions on transport and retention of phosphate by *Escherichia coli*', *J. Bacteriol*., 1982, **152**, pp. 7–13

© The Institution of Engineering and Technology 2013